Exciton Binding Energy in Organic-Inorganic Tri-Halide Perovskites

Abdelrahman M. Askar*[1] and Karthik Shankar[1,2]

[1]*Department of Electrical and Computer Engineering, University of Alberta, Edmonton, Alberta, T6G 1H9, Canada*

[2]*National Institute for Nanotechnology, National Research Council, Edmonton, Alberta, T6G 2M9, Canada*

*E-mail: aaskar@ualberta.ca

Abstract

The recent dramatic increase in the power conversion efficiencies of organic-inorganic tri-halide perovskite solar cells has triggered intense research worldwide and created a paradigm shift in the photovoltaics field. It is crucial to develop a solid understanding of the photophysical processes underlying solar cell operation in order to both further improve the photovoltaic performance of perovskite solar cells as well as to exploit the broader optoelectronic applications of the tri-halide perovskites. In this short review, we summarize the main research findings about the binding energy of excitons in tri-halide perovskite materials and find that a value in the range of 2-22 meV at room temperature would be a safe estimate. Spontaneous free carrier generation is the dominant process taking place directly after photoexcitation in organic-inorganic tri-halide perovskites at room temperature, which eliminates the exciton diffusion bottleneck present in organic solar cells and constitutes a major contributing factor to the high photovoltaic performance of this material.

*To whom correspondence should be addressed

Keywords: Perovskite Solar Cells, Exciton Binding Energy, Organic-Inorganic Tri-Halide Perovskite, Magneto-Absorption, Photoluminescence, THz Spectroscopy, Nano-Perovskite, Dielectric Constant.

CONTENTS

1 INTRODUCTION

Over the last 3 years, the photovoltaics research community has witnessed an

unprecedented breakthrough in the field of hybrid solar cells based on organic-inorganic tri-halide perovskite as the light absorbing semiconductor, to the extent that many scientists nowadays believe that we are living in the '***Perovskite Era***'. This revolution has been driven by the compelling need for low cost and high efficiency solar cells, which seems to be readily achievable by perovskite solar cells (PSCs) that have already exhibited certified power conversion efficiencies (PCE) close to and exceeding 20%.[1–4]

When first introduced, PSCs were designed to follow the excitonic solar cell concept, in which absorbing nanoscale perovskite crystals (instead of a dye) sensitized the surface of an electron-transport layer such as mesoporous TiO_2 and a hole transport layer was then infiltrated into the sensitized TiO_2.[5–7] Later on, it was found that PSCs also work in planar configurations, similar to those used in thin film semiconductor solar cells, with comparable efficiencies.[8] Despite the outstanding success of PSCs in a relatively short time frame, several fundamental questions remain to be fully understood with regard to the photophysics of PSCs. Some material properties are reported throughout the literature with a wide range of values, while operating mechanisms of the perovskite solar cell device remain controversial, awaiting further studies to confirm or negate currently available proposals.

To help researchers be on top of all these rapid advancements and recent updates related to this revolutionary class of material from different aspects and its many applications, review articles and perspectives[9–36] are necessary to make it easier for the perovskite research community to be aware of all the corresponding details and how different studies relate to each other and illustrate the discrepancies in the findings of various related studies, if any.

Among the open questions in the PSC operation is the value of the exciton binding energy. In general, upon light absorption, species called excitons are generated, which are simply bound

states of electron-hole pairs due to coulombic attraction.[37] In inorganic solar cells, due to the high permittivity and low effective mass of the semiconductors typically used, the binding energy of these excitons (called Wannier-Mott excitons) is very small (a few meV),[38] which is less than the thermal energy at room temperature (25 meV), due to which Wannier-Mott excitons are dissociated instantaneously to free charge carriers. In organic semiconductors, on the other hand, the exciton binding energy is relatively high (around 1 eV) due to the correspondingly low permittivity and high effective mass. The understanding of the exciton nature within the PSC and its binding energy are crucial for further development of high efficiency terrestrial solar cells, space solar cells, photodetectors, non-linear optical devices, etc. It is important to know whether free charges are generated upon excitation, or rather excitons are produced which dissociate either in the perovskite layer or at the heterojunction interface.

1.1 Exciton Binding Energy in PSCs

There has been a dispute in the perovskite research community in estimating the exact value for the binding energy of excitons in PSCs, and values ranging from 2 meV to 55 meV have been reported.[39–51] A variety of spectroscopic techniques have been exploited leading to different conclusions, to the extent that some researchers in their recent work invalidated their own previous research findings.[41, 52, 53] This disagreement between reported values is not only due to using different techniques and how the results are interpreted, but also due to differences in the quality of the perovskite material being studied.

1.2 The Contribution

In this mini-review, we try to summarize different pieces of evidence from the literature to understand the exciton nature in PSCs and the origin of dispute in the reported values.

2 EARLIER STUDIES

The study of different materials belonging to the family of organic-inorganic lead tri-halide perovskites, especially methylamonium (MA) lead iodide (bromide), dates back to the 1980s.[54] Those earlier studies focused primarily on studying the crystal structure, energy band, and related parameters such as the Bohr radii, binding energies, reduced masses, and oscillator strengths of the excitons in this family of crystals.

2.1 Magneto-absorption (MA) and luminescence studies

Forming some of the earliest studies, Hirasawa et al.[55] investigated the magneto-absorption spectra of the lowest energy exciton in $MAPbI_3$ at magnetic fields up to 40 T at a constant temperature of 4.2 K. In conjunction with the optical studies, the researchers extracted an exciton binding energy (R*) of 37 meV for $MAPbI_3$ synthesized from MAI and PbI_2 in acetonitrile solution, which resulted in microcrystals of perovskite. The accuracy of this R* value was doubtful due to the magnetic-field induced photoluminescence (PL) which the MA spectra suffered from. Using the same synthesis procedure of $MAPbI_3$ and in the same year, Ishihara[56] reported a study on the temperature dependence of luminescence for $MAPbI_3$, from which an R* value of 45 meV was estimated. Nine years later, Tanaka and co-workers[57] re-measured the MA spectra of a randomly oriented polycrystalline $MAPbI_3$ film on a quartz substrate with a higher accuracy than the earlier mentioned study. This time, the researchers first compared the optical properties of their perovskite film to single crystal samples before doing MA measurements on the film to confirm that the optical properties were the same, and their measurements gave the intrinsic value for R*, which they estimated to be 50 meV. This was based on the exciton diamagnetic coefficient measurement in MA spectra, and subsequently calculating the binding energy based on the hydrogenic model. The main concern with those reported R* values, extracted from the MA spectra presented earlier, was the assumption of a magnetic field independent R*, which was found to be an inaccurate

assumption.[41] Moreover, the high frequency dielectric constant (ε_∞) used in the calculations of R* was only a choice of the model used by the researchers and not experimentally determined.[58] In the next section, we will shed light on more recent experimental investigations as well as theoretical calculations of the exciton binding energy, aiming to get a more in-depth understanding of the fundamental photophysical processes in the perovskite material related to the solar cell operation.

3 RECENT STUDIES

It was not until the recent surge in high efficiency PSCs that researchers started to inquire again into the reported values of R^* in halide perovskite films.

3.1 Optical absorption studies

Petrozza et al.[52] estimated R* using the temperature-dependent absorption linewidth of the observed excitonic transitions in polycrystalline films of $CH_3NH_3PbI_{3-x}Cl_x$ and $CH_3NH_3PbI_3$. Fig. 1 shows the corresponding results, where the sharp peaks at lower temperatures were attributed to an excitonic transition.

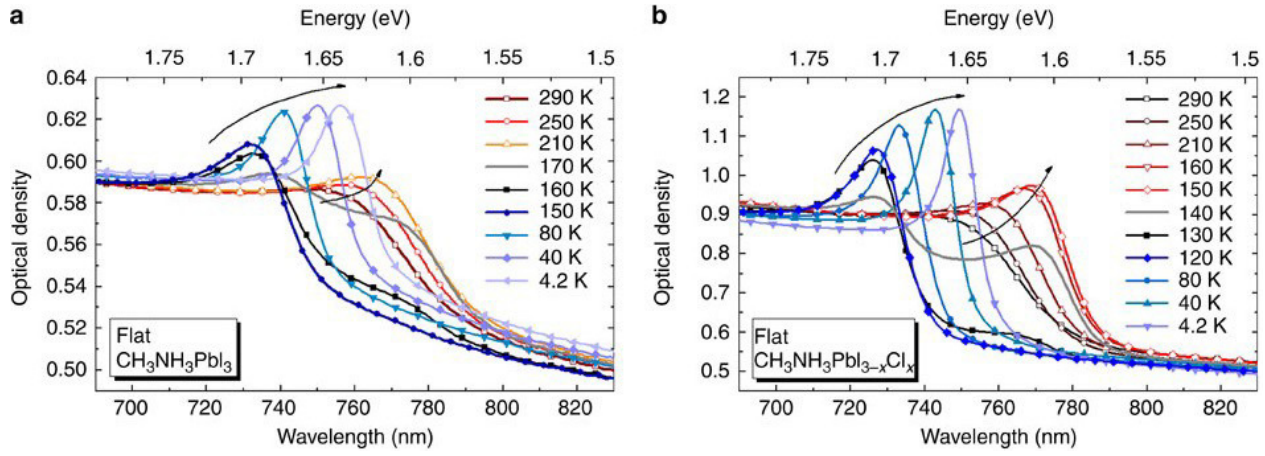

Figure 1. (a) Temperature dependence (290 - 4.2 K) of the absorption spectra for $CH_3NH_3PbI_3$ and (b) $CH_3NH_3PbI_{3-x}Cl_x$. Reprinted with permission from **ref. 47,** V. D'Innocenzo, G. Grancini, M. J. P. Alcocer, A. R. S. Kandada, S. D. Stranks, M. M. Lee, G. Lanzani, H. J. Snaith, and A. Petrozza, Excitons versus free charges in organo-lead tri-halide perovskites. *Nat Commun* 5, 582–587 (**2014**). Copyright@Nature Publishing

Group.

At a temperature of ~ 170 K, the evolution of a second peak is observed, which is mostly due to the phase transition in perovskite from orthorhombic to tetragonal around this temperature.[59, 60] Based on this experimental data, Petrozza and co-workers estimated an R* value of 55 ± 20 meV in $CH_3NH_3PbI_{3-x}Cl_x$ perovskite, and the corresponding value of R* in the $CH_3NH_3PbI_3$ film was missing and not reported. The problem with this estimation of R* is the assumption of a temperature-independent value, which turned to be inaccurate.[41] Another key finding from the researchers was that under PV operating conditions, free charge carriers are predominant over excitons after photoexcitation at room temperature, whereas at low temperatures (LTs) (specifically below 120 K) the exciton population becomes dominant over free charge carriers. A theoretical calculation of R* using density functional theory (DFT) in $CH_3NH_3PbI_3$ predicts a value of 48 meV[61] based on the Wannier-Mott model with ε_∞. Nevertheless, in the case of a sufficiently long exciton lifetime (which is the case in $CH_3NH_3PbI_3$), this result of 48 meV for R* is inaccurate and overestimated, requiring the R* value to be recalculated.[61]

3.2 Revisited magneto-absorption and optical absorption results

By reexamining Fig. 1, we notice that the excitonic peak is clearly visible in the absorption spectrum in the LT regime, but the same is not true at room temperature (RT). Recently, the results of many studies[53, 62] on tri-halide perovskites carried out at RT were analyzed in the context of free charge carrier transport, although if the previously reported values of R* at LT (37-50 meV) are the same at RT, we would expect both free charge carriers and excitons to co-exist.[63] Even et al.[63] carried out a theoretical investigation by making use of, and modeling, recent and old experimental data aiming for a better understanding of the exciton nature in lead iodide and mixed-halide perovskite, especially at RT. Following a rigorous analysis, Even and co-workers[63] found that

optical absorption results from Ishihara[56] are best described through calculations assuming a higher effective dielectric constant (ε_{eff}) than the high frequency permittivity (ε_{∞}) arbitrarily chosen by Ishihara and co-workers. The higher ε_{eff} used in the calculations by Even et al.[63] was attributed to a screening effect induced by vibrations at LT, which led to an estimation of R* in the range of 18-24 meV instead of 37-50 meV at a temperature of 5 K. On the other hand, at RT, an even higher ε_{eff} was used in the estimation of R*, leading to a value of 5 meV down-shift in the binding energy from the previous estimate of 15 meV. The higher ε_{eff} at RT was attributed to collective tumbling of the cation's C-N axis in the perovskite compound.[63] Fig. 2 shows the good agreement between both measured and calculated optical absorption spectra assuming higher ε_r in the calculations for two different temperatures.[63]

3.3 Temperature-dependent PL

Following another technique to estimate R*, Sun and colleagues[64] used temperature-dependent PL intensities from a solution processed $CH_3NH_3PbI_3$ film with a least square fit of the data to the Arrhenius equation, which led to an R* value of 19 ± 3 meV (Fig. 3).

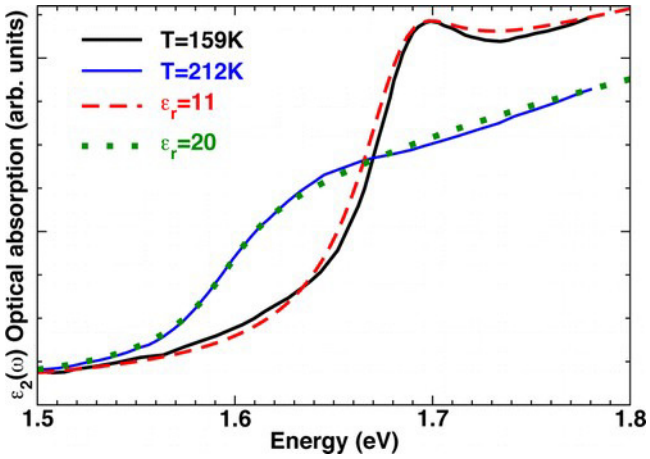

Figure 2. Optical absorption spectra for $CH_3NH_3PbI_3$. Experimental data (solid lines) taken from Ishihara's paper,[56] simulation results based on theoretical calculations (dashed lines) of absorption spectra[63] for different effective dielectric constants (ε_{eff}). Reprinted with permission from **ref. 63,** J. Even, L. Pedesseau, and C. Katan, Analysis of Multivalley and Multibandgap Absorption and Enhancement of Free Carriers

Related to Exciton Screening in Hybrid Perovskites. *J. Phys. Chem. C* 118, 11566–11572 (**2014**). Copyright@American Chemical Society.

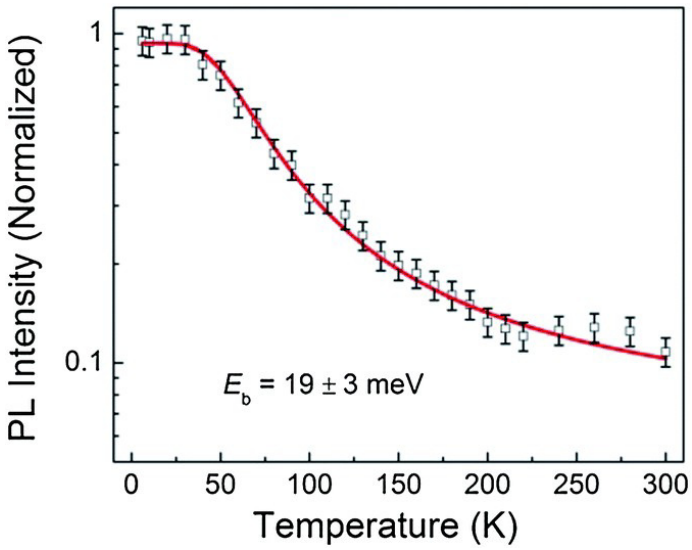

Figure 3. Temperature-dependent integrated PL intensity of the $CH_3NH_3PbI_3$ film under excitation of a 532 nm continuous-wave laser beam. The solid line is the best fit based on the Arrhenius equation. Reprinted with permission from **ref. 64,** S. Sun, T. Salim, N. Mathews, M. Duchamp, C. Boothroyd, G. Xing, T. C. Sum, and Y. M. Lam, The origin of high efficiency in low-temperature solution-processable bilayer organometal halide hybrid solar cells. *Energy Environ. Sci.* 7, 399–407 (**2014**). Copyright@Royal Society of Chemistry.

This estimation does not use any model of the exciton states and fits well with values of R* presented earlier using higher ε_r in addition to other recent calculations.[58] The authors have listed this relatively low R* they estimated as one of the origins behind high performance PSCs, nevertheless, they insisted still on the importance of an electric field to dissociate all the excitons generated, in addition to the energy offset at the heterointerface between the perovskite film and electron- or hole-transporting layers.

3.4 Optical and dielectric constants of $CH_3NH_3PbI_3$ high quality film

At this point, it is of interest to show recent experimental data which has been used to determine the optical and dielectric constants in $CH_3NH_3PbI_3$ film and show the implications of these results on the estimation of R*. Lin et al.[39] used a combination of spectroscopic ellipsometry, total transmittance, and near-normal incidence reflectance measurements to determine these

properties. Fig. 4 shows the real (n) and imaginary (k) components of the refractive index, from which the complete dielectric constant including both the real (ε') and imaginary (ε'') components, are calculated for the high frequency regime, which fits quite well with other reported data.[65, 66] More interestingly, the researchers were able to measure ε' and ε'' at low frequency using a combination of impedance analysis and charge extraction by linearly increasing voltage (CELIV) techniques, leading to an estimate of 70 for the static dielectric constant (ε_s). As highlighted earlier, the use of ε_∞ in estimating R* is inaccurate, which is due to the fact that exciton radius is larger compared to the lattice constant in tri-halide perovskites, and therefore using ε_s will give more accurate results.[39, 66] Using a value for ε_s of 70, Lin et al.[39] recalculated R* based on the magneto-optical approaches of Tanaka[57] and others[55, 67] and found R* ≈ 1.7–2.1 meV.

3.5 Results from THz spectroscopy

In order to truly reveal the intrinsic nature of excitons in perovskite, it would be advantageous to observe the dynamics of excitons using a real-time spectroscopy technique in a single crystal, rather than in a film. That is exactly what Cooke et al.[68] did when they studied a large single crystal $CH_3NH_3PbI_3$ perovskite using the transient multi-THz spectroscopy to investigate the intrinsic mobile charge generation dynamics. In other words, they used ultra-broadband THz pulses (4 - 135 meV) to measure the complex dielectric function in the single crystal perovskite. One major finding of this study is the observation of a short-lived intra-excitonic transition accompanied with R* of the order of 17 meV at RT under high pump fluence. More interestingly, the signature of the exciton is found to disappear on a 1 ps time scale, leading to mobile charge carriers.

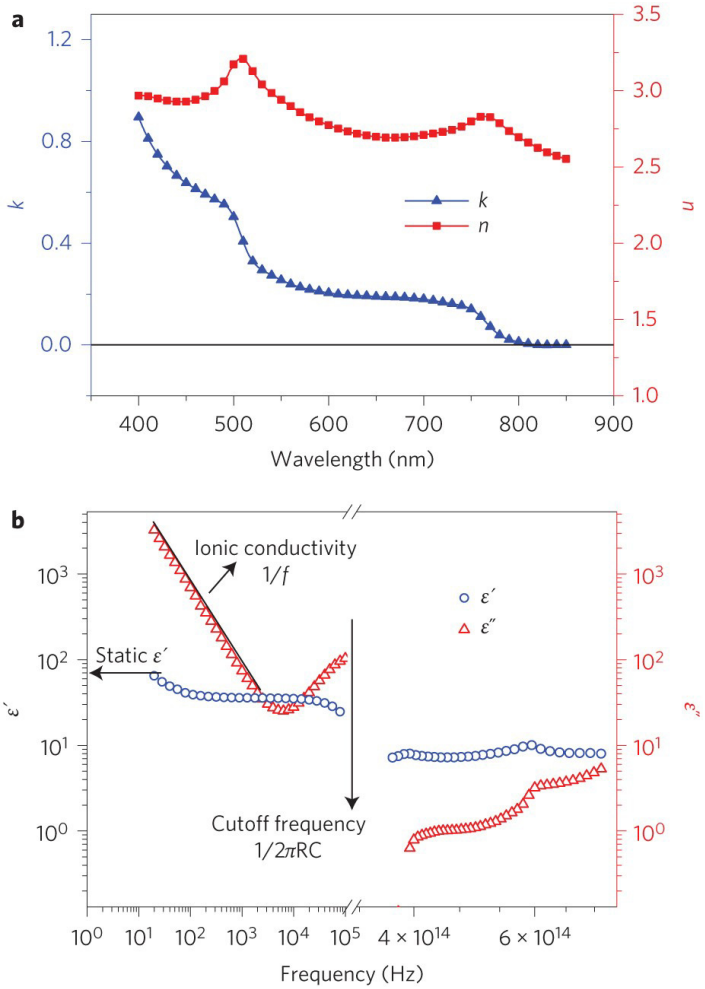

Figure 4. (a) Optical constants of the $CH_3NH_3PbI_3$: refractive index (n) and extinction coefficient (k), as determined by employing spectroscopic ellipsometry, near-normal incidence reflectance and total transmittance; (b) Dielectric constants of $CH_3NH_3PbI_3$, real and imaginary parts, in the optical (high) frequency regime as determined from n, k and low-frequency and static values from impedance analysis and CELIV, respectively. Reprinted with permission from **ref. 39,** Q. Lin, A. Armin, R. C. R. Nagiri, P. L. Burn, and P. Meredith, Electro-optics of perovskite solar cells. *Nat Phot.* 9, 106–112 (**2015**). Copyright@Naure Publishing Group.

Using similar THz spectroscopy techniques, Douhal et al.[69] studied another member of the perovskite family, namely formamidinium (FA) lead tri-iodide perovskite, and they reached the same conclusion regarding the dissociation of exciton, which can be summarized in Fig. 5. Although the analysis of the THz kinetics revealed two different rising components (time constants) in this study of the $FAPbI_3$, it was found that the major part of the mobile charge carrier population in the film was formed within ~ 1 ps (comparable to temporal resolution in the THz

spectroscopy setup), which agrees perfectly with the THz results presented above. The difference in the THz conductivity rise times was attributed to the dissociation of excitons with different R* values. The importance of this study is that it demonstrated the findings of the results previously reported for $MAPbI_3$ to be of general relevance to the broader family of organic-inorganic tri-halide perovskites.

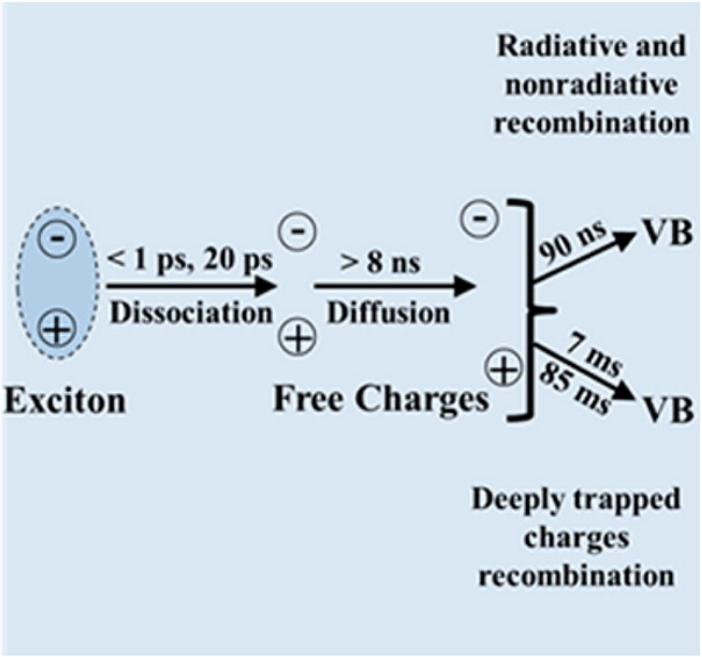

Figure 5. Schematic representation showing the exciton dissociation process, charge carrier diffusion, radiative and nonradiative recombination, and the recombination of deeply trapped charges in the studied $FAPbI_3$ film. Reprinted with permission from **ref. 69**, P. Piatkowski, B. Cohen, C. S. Ponseca Jr., M. Salado, S. Kazim, S. Ahmad, V. Sundstrom, and A. Douhal, Unraveling Charge Carriers Generation, Diffusion, and Recombination in Formamidiniurn Lead Triiodide Perovskite Polycrystalline Thin Film. *J. Phys. Chem. Lett.* 7, 204–210 (**2016**). Copyright@American Chemical Society.

3.6 Very high-field interband magneto-absorption study

Although magneto-absorption studies were amongst the very early techniques to study excitons in perovskite materials, a recent study by Miyate et al.[41] which used a very high magnetic field revealed new findings. Studying a 300-nm-thick polycrystalline film of $CH_3NH_3PbI_3$ deposited directly on a glass substrate, the authors were able to estimate R* = 16 ± 2 meV at LT. Of more interest to practical device applications, R* at RT is found in the study to collapse to only

a few meV, again suggesting spontaneous free carrier generation upon light absorption in the perovskite film.[41] One main reason making this study more accurate over previous magneto-absorption studies is the fact that its estimation of R* is independent of any assumed values of effective mass or dielectric constant, which was a major source of uncertainty in previous estimates of R* based on magneto-absorption spectra. In Fig. 6, the magnetic field-dependent optical density spectra are depicted for the perovskite film. The main peak near 1.6 eV stems from a hydrogen-like 1s exciton transition, while at higher energies a free-carrier behavior is observed with a series of interband transitions.

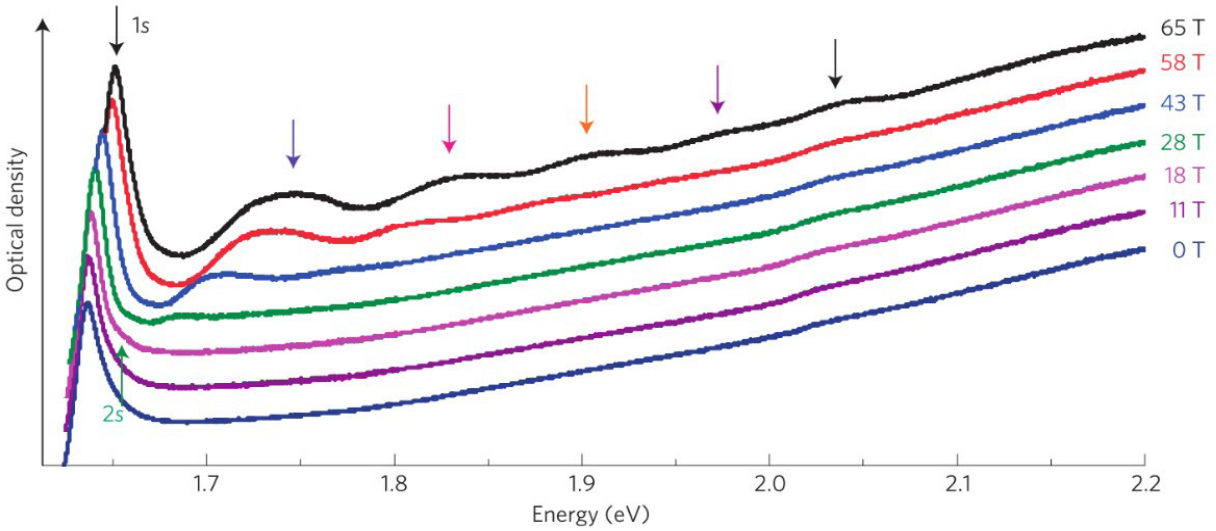

Figure 6. Magnetic field dependence (0 - 65 T) of the optical density for the perovskite $CH_3NH_3PbI_3$ film. The optical density spectra is measured during a single long (500 ms) pulse of the magnetic field. The spectra are offset for easier comparison. Reprinted with permission from **ref. 41**, A. Miyata, A. Mitioglu, P. Plochocka, O. Portugall, J. T.-W. Wang, S. D. Stranks, H. J. Snaith, and R. J. Nicholas, Direct measurement of the exciton binding energy and effective masses for charge carriers in organic-inorganic tri-halide perovskites. *Nat. Phys.* 11, 582–587 (**2015**). Copyright@Nature Publishing Group.

The previous results are extended further by another study published recently by Galkowski et al.[70] using the same magnetoabsorption/transmission technique to show that an R* in the range of 14 – 24 meV at LT is an accurate estimate which applies to the broader family of organic-inorganic tri-halide perovskite semiconductors. This includes $MAPbI_3$, $MAPbBr_3$, and their

formamidinium (FA) analogies, i.e., $FAPbI_3$ and FA $PbBr_3$. Again, these values of R* drop significantly at RT.

3.7 Other studies

For the sake of completeness, results from a few other main studies on excitons in perovskite are briefly summarized next. Through the analysis of monomolecular, bimolecular, and trimolecular (Auger) recombination rate constants, Beard et al.[43] estimated R* ~ 13 meV in $CH_3NH_3PbI_3$ films. Although they did not estimate an exact value of R*, Herz and co-workers [53] interpreted the shape of their transient THz spectra obtained from a perovskite film to be due to free charge carriers rather than excitons, and that an exciton binding energy of ~ 40 meV would not be able to explain their observations of the spectra, again suggesting a lower exciton binding energy with spontaneous free charge carrier generation. Most of the studies focused on the iodide member ($CH_3NH_3PbI_3$) of the organic-inorganic lead halide family or its hybrid ($CH_3NH_3PbI_{x-3}Cl_x$) version due their importance for high efficiency PSCs. Nevertheless, the wide band gap members of the family, i.e., $CH_3NH_3PbBr_{x-3}Cl_x$ and $CH_3NH_3PbCl_3$, were found to be important in many optoelectronic applications [44–46] and an R* of ~ 50 meV was estimated in $CH_3NH_3PbCl_3$ thin films.[71]

Also, other studies focused on studying the ultra-fast transient absorption (TA) spectra of perovskite films to unravel the exciton dynamics.[72–74] The common theme of the results from these studies elucidate that the exciton diffusion into free charge carriers occurs essentially in the sub-picosecond time scale. Nevertheless, these TA studies ignore one important aspect of the studied perovskite films which is the polycrystalline nature of these films due to the distinct crystalline grains. That is what Simpson et al.[75] investigated by studying the spatial and temporal ultrafast charge carrier dynamics using femtosecond TA microscopy (fs-TAM). One of the most exciting

findings of this study is that the TA dynamics extracted from the fs-TAM images were found to be extremely sensitive to the spatial position probed within the perovskite film.[75] Fig. 7 shows the fs-TAM images for pristine perovskite films and two different perovskite composites. What is important to notice is the change of the sign of the TA observed signals (positive indicates more probe light reaching the detector, while negative corresponds to excited-state absorption)[75] over the sample spatial position. From the TAM results, Simpson et al.[75] deduced the coexistence of excitons and free charge carriers under high photoexcitation fluences.

Other important parameters, which are often less studied within the context of investigating the exciton dynamics, are the effects of sub-bandgap states as well as the density of photoexcited charges. That is why some studies focused on probing the charge carrier dynamics in the perovskite film and the modeling of these phenomena under variable excitation fluences.[69, 74, 76, 77] For instance, Stranks and co-workers[77] were successful in developing a theoretical model and verified it experimentally to describe the interplay between excitons, free charges, and electronic subgap states. Interestingly, they found that under solar-cell operation conditions the fraction of free charge carriers versus excitons would be increased towards 100% by reducing the photodoping density, which is considered to be the case due to the existence of subgap states.[78] In other words, the increase in photoexcited charge density leads to a reduction in the density of available trap states, and to an increase in the fractional time the charges spend as excitons.

It is worth mentioning here that the exact R* value is expected to vary from one study to another simply due to the low ambient stability of materials which may introduce a source of error in optical measurements widely used to estimate R*. Moreover, theoretical and experimental techniques used for estimating R*, developed originally for inorganic semiconductors, may not be adequate to accurately enough extract R* in these organic-inorganic hybrid perovskite materials.[79]

Also, it should be noted that exciton characteristics are sensitive to parameters such as the method of synthesis and structural details, which clearly differ, even if little, from one study to another leading to unavoidable discrepancies between reported values.

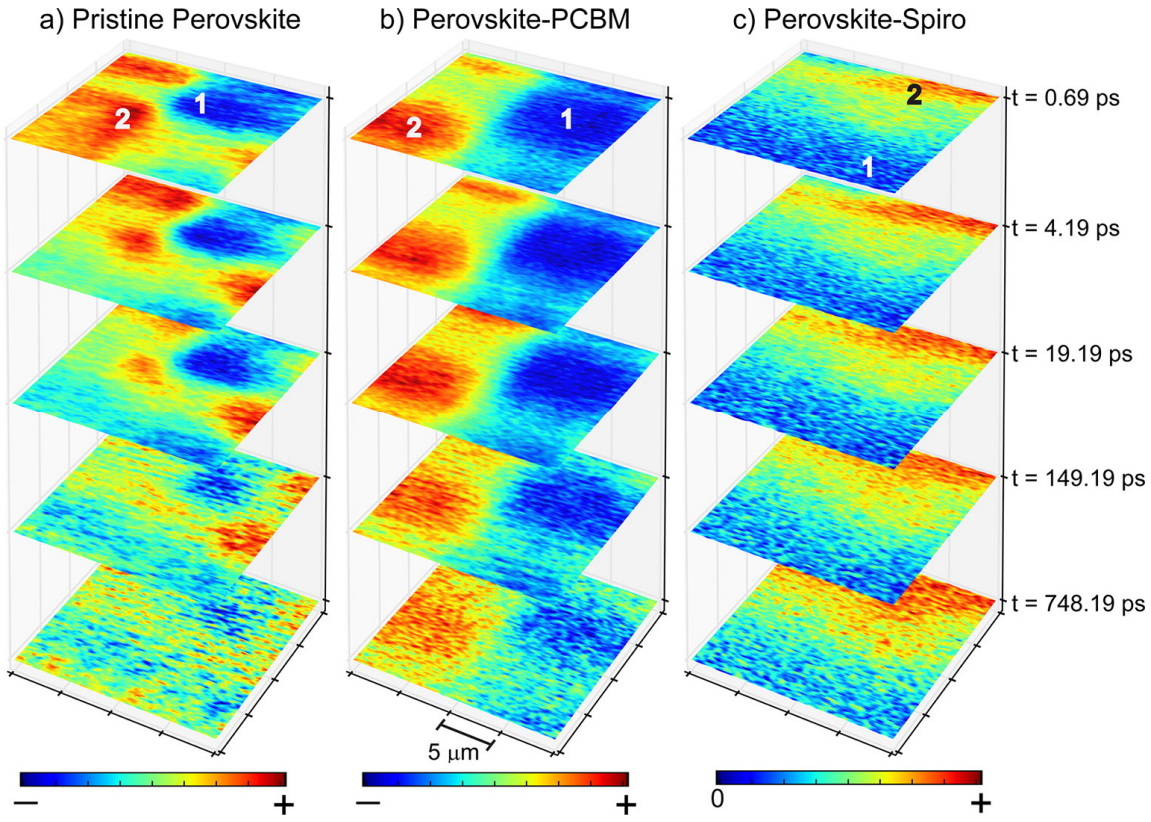

Figure 7. fs-TAM images taken for the same are in (a) pristine perovskite, (b) perovskite-PCBM, and perovskite-Spiro-OMeTAD films at different delay times. Reprinted with permission from **ref. 75**, M. J. Simpson, B. Doughty, B. Yang, K. Xiao, and Y.-Z. Ma, Spatial Localization of Excitons and Charge Carriers in Hybrid Perovskite Thin Films. *J. Phys. Chem. Lett.* 6, 3041–3047 (**2015**). Copyright@American Chemical Society.

4. THE EFFECT OF THE HALIDE ON EXCITON BINDING ENERGY

In this section, the effect of the halide component of the $CH_3NH_3PbX_3$ perovskite (X = Cl, Br, I) on R* is briefly highlighted. First, Fig. 8 shows the effect of the halide in the $CH_3NH_3PbX_3$

system on the exciton peak position in the absorption spectra (400 nm for X = Cl, 530 nm for X = Br, 770 nm for X = I).[80]

The fundamental electronic structures for all three halides are essentially the same, with a blue-shift of the whole structure for a substitution with a smaller halogen atom. Nevertheless, the dielectric constant gets reduced with a smaller halogen atom which leads to reduced dielectric screening of the Coulomb interaction between the electrons and holes. Tanaka et al.[57] compared R* for $CH_3NH_3PbBr_3$ and $CH_3NH_3PbI_3$ based on MA spectra of both, and estimated an R* of 76 meV and 50 meV, respectively. The same behavior was observed by Beard and co-workers[81] as they estimated R* of ~ 13 meV and ~ 40 meV in $CH_3NH_3PbI_3$ and $CH_3NH_3PbBr_3$ thin films, respectively.

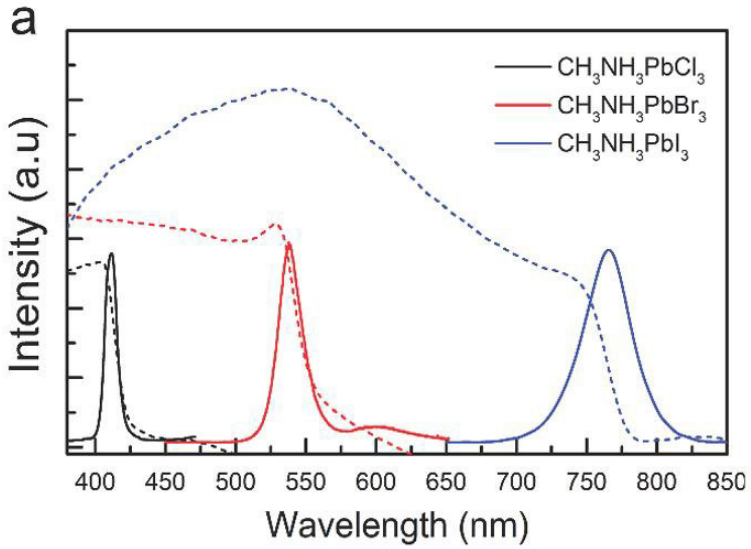

Figure 8. Optical absorption (dashed lines) and room temperature PL (solid lines) of $CH_3NH_3PbX_3$ (X = Cl, Br, I) platelets. Reprinted with permission from **ref. 80**, S. T. Ha, X. Liu, Q. Zhang, D. Giovanni, T. C. Sum, and Q. Xiong, Synthesis of Organic–Inorganic Lead Halide Perovskite Nanoplatelets: Towards High-Performance Perovskite Solar Cells and Optoelectronic Devices. *Adv. Opt. Mater.* 2, 838–844 (**2014**). Copyright@WILEY Publishing Group.

In the mixed halide case, i.e., $CH_3NH_3PbI_{3-x}Cl_x$, an R* of 62.3 ± 8.9 meV was estimated using low temperature PL, which is higher than reported values for $CH_3NH_3PbI_3$ and is attributed

to Cl substitution and the resulting hindered collective molecular motions, leading to higher R*. Using the fitting of integrated PL spectra, another R* value of 98 meV for $CH_3NH_3PbI_{3-x}Cl_x$ was reported[50] which could be different from the previous value (62 meV) due changes in the composition.

5. EXCITON BINDING ENERGY IN NANO-PEROVSKITES

The discussion so far concerning R* has focused on 3D lead tri-halide perovskite systems (perovskite microcrystallites also represent 3D/bulk properties). Nevertheless, the study of low dimensional, i.e., 2D, 1D, and 0D, similar perovskite systems and the corresponding R* in these systems have been also of interest since the early 1990s[50, 82–84]. That is mainly due to the enhanced R* in these low-dimensional systems when compared to the corresponding 3D ones. For instance, using semi-empirical as well as *ab initio* band-structure calculations, Koutselas et al.[50] estimated an R* in the range of few hundreds of meV for 2D, 1D, and 0D lead iodide systems, an order of magnitude higher than in the 3D case. In these calculations, ε_∞ was again adopted and a good agreement was found between both calculated and experimentally estimated values of R* based on available experimental data by that time.

Along with the intensive research being done on PSCs recently, there has been a revived interest in studying nano-perovskites, e.g., perovskite nanoparticles and nanoplatelets, examining their electronic properties, including the determination of R*, as well as investigating the applications of these perovskite-based nanomaterials.[48, 79, 80, 85–94] To compare the electronic properties of organic-inorganic lead tri-bromide ($CH_3NH_3PbBr_3$) nanocrystals (NCs) in contrast to bulk crystals (BCs), Zheng and co-workers[48] applied temperature dependent photoluminescence measurements and X-ray spectroscopy techniques to study both perovskite NCs and BCs which,

for instance, revealed R* of 0.32 ± 0.10 eV for NCs versus 0.084 ± 0.010 eV for the BCs. Fig. 9 shows the UV-Vis absorption spectra of $CH_3NH_3PbBr_3$ in 3D (bulk) and 0D configurations.[85] In the 3D case, $CH_3NH_3PbBr_3$ exhibits an excitonic peak at 546 nm, where for the 0D (nanoparticle) case, the excitonic peak is observed at 527 nm.

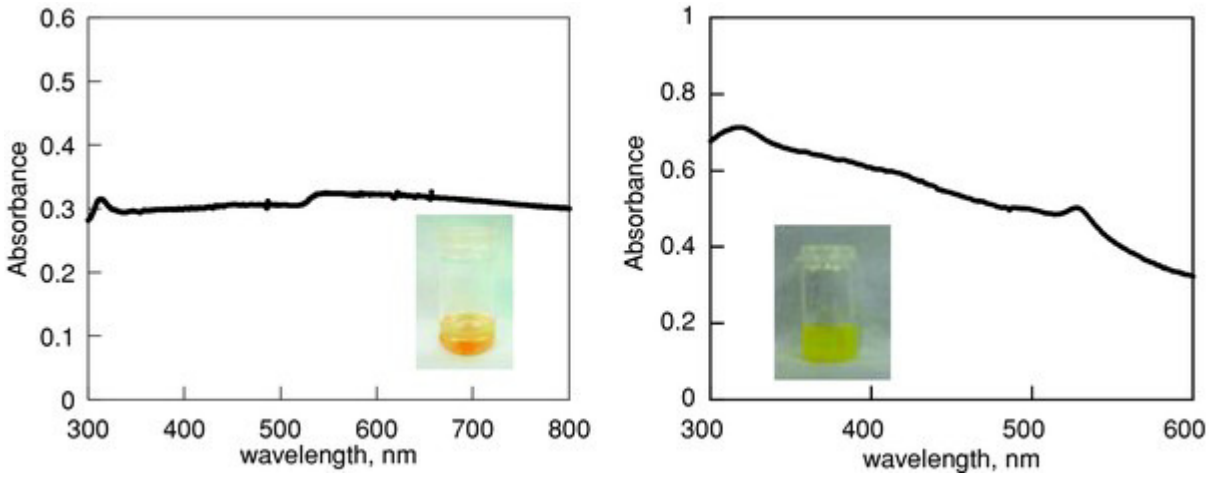

Figure 9. UV-Vis absorption spectra of $CH_3NH_3PbBr_3$ in toluene, left) bulk 3D material, right) 0D material (nanoparticle). Reprinted with permission from **ref. 85**, L. C. Schmidt, A. Pertegás, S. González-Carrero, O. Malinkiewicz, S. Agouram, G. M. Espallargas, H. J. Bolink, R. E. Galian, and J. Pérez-Prieto, Nontemplate Synthesis of $CH_3NH_3PbBr_3$ Perovskite Nanoparticles. *J. Am. Chem. Soc.* 136, 850–853 (**2014**). Copyright@American Chemical Society.

Due to the high R* values in these nano-perovskite systems which result from quantum size effects[88] and the concomitantly high PL quantum yield[85], it was intuitive to exploit these nano-perovskites in light emission applications such as light emitting diodes (LEDs) and lasers.[95–98] The main reason for this enhanced R* in perovskite nanostructures, as for other semiconductors, is the weaker dielectric screening effect when compared to the bulk materials. In bulk perovskite, which has a large dielectric constant,[99] the Coulomb interaction is highly screened between electrons and holes, leading to reduced R*, where in nanostructures, the dielectric constant gets reduced leading to lowered screening between electrons and holes, and consequently, higher R*. Also, these perovskite nanostructures found their way into high efficiency PSCs. Park et al.[100] reported a

$CH_3NH_3PbI_3$ nanowire perovskite solar cell with the best performing device delivering a PCE of 14.71% (not an optimized device) at standard AM 1.5G solar illumination. Fig. 10 shows a TOC figure from the above mentioned paper, highlighting the perovskite NW, PSC device structure, and the achieved performance. This outstanding performance was attributed to the enhanced hole injection from perovskite to the hole transport layer (HTL) in addition to the higher lateral conductivity of nanowire film.

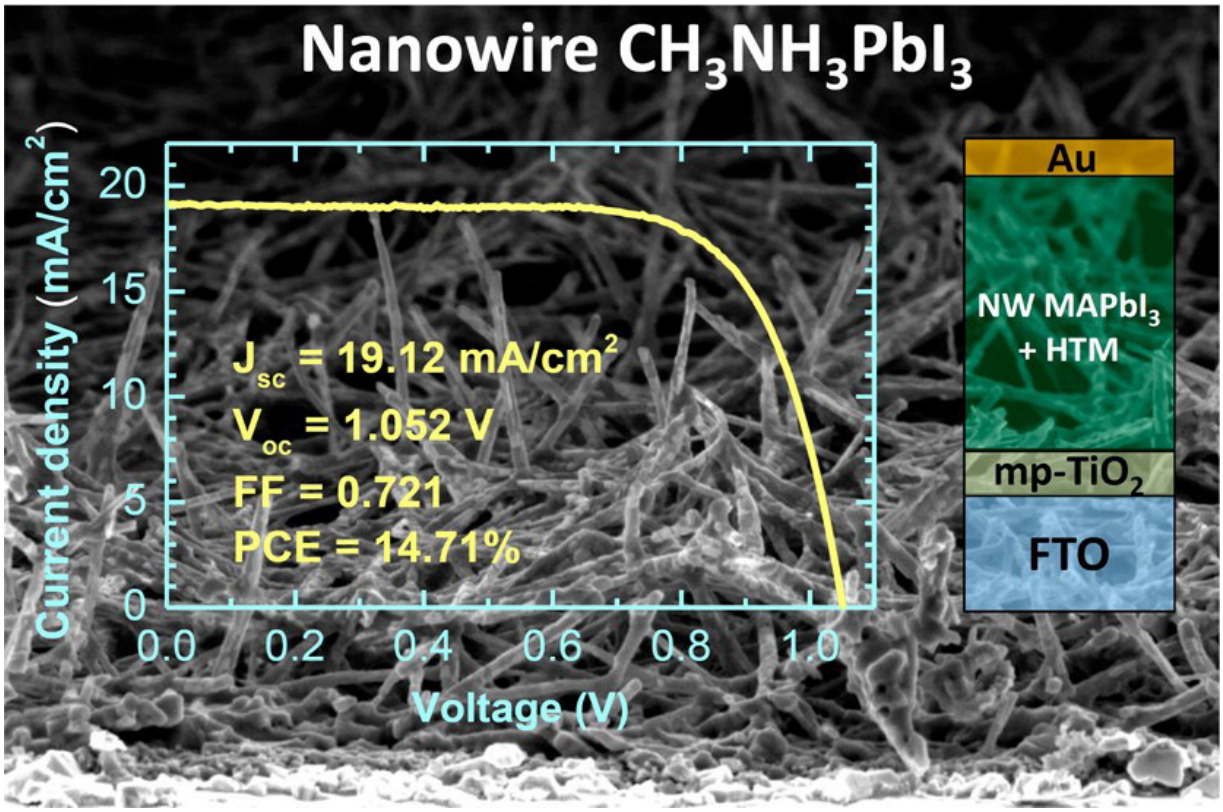

Figure 10. TOC graphic from Park et al.[100] showing SEM image of the perovskite nanowires, with the PSC device structure and the corresponding J/V performance and main cell parameters. Reprinted with permission from **ref. 100**, J.-H. Im, J. Luo, M. Franckevičius, N. Pellet, P. Gao, T. Moehl, S. M. Zakeeruddin, M. K. Nazeeruddin, M. Grätzel, and N.-G. Park, Nanowire Perovskite Solar Cell. *Nano Lett.* 15, 2120–2126 (**2015**). Copyright@American Chemical Society.

6. CONCLUSION

In summary, the exciton binding energy in organic-inorganic tri-halid perovskite is clearly difficult

to measure directly and has been a matter of intense debate, with values reported in the literature covering a broad range from 2 to 55 meV. The very early studies using magneto-optical spectra estimated values of R* around 45 meV using ε_∞ in the calculations. More recent studies using a wide variety of techniques suggest lower R* with values from 2 to 22 meV at RT for the $MAPbI_3$, which is more accurate. Despite the exact value of R*, there is a growing agreement between the studies on the idea of spontaneous free charge carrier generation after photoexcitation in the perovskite within the timescale of a couple of picoseconds, which in turn makes the operation of a PSC predominantly non-excitonic. This conclusion is considered one of the main reasons behind the spectacular performance of PSCs.

Acknowledgements: The authors thank NSERC and NRC-NINT for funding support. A. Askar acknowledges scholarship support from Alberta Innovates Technology Futures and thanks Prof. Jillian Buriak for helpful discussions.

References and Notes

1. W. S. Yang, J. H. Noh, N. J. Jeon, Y. C. Kim, S. Ryu, J. Seo, and S. I. I. Seok. High-performance photovoltaic perovskite layers fabricated through intramolecular exchange. *Science* 348, 1234–1237 (**2015**).

2. W. Chen, Y. Wu, Y. Yue, J. Liu, W. Zhang, X. Yang, H. Chen, E. Bi, I. Ashraful, M. Grätzel, and L. Han. Efficient and stable large-area perovskite solar cells with inorganic charge extraction layers. *Science* 350, 944–948 (**2015**).

3. N. J. Jeon, J. H. Noh, W. S. Yang, Y. C. Kim, S. Ryu, J. Seo, and S. I. I. Seok. Compositional engineering of perovskite materials for high-performance solar cells. *Nature* 517, 476–480 (**2015**).

4. H. Zhou, Q. Chen, G. Li, S. Luo, T. Song, H.-S. Duan, Z. Hong, J. You, Y. Liu, and Y. Yang. Interface engineering of highly efficient perovskite solar cells. *Science* 345, 542–546 (**2014**).

5. H.-S. Kim, C.-R. Lee, J.-H. Im, K.-B. Lee, T. Moehl, A. Marchioro, S.-J. Moon, R.

Humphry-Baker, J.-H. Yum, J. E. Moser, M. Grätzel, and N.-G. Park. Lead Iodide Perovskite Sensitized All-Solid-State Submicron Thin Film Mesoscopic Solar Cell with Efficiency Exceeding 9%. *Sci. Rep.* 2, 591 (**2012**).

6. J. Burschka, N. Pellet, S.-J. Moon, R. Humphry-Baker, P. Gao, M. K. Nazeeruddin, and M. Gratzel. Sequential deposition as a route to high-performance perovskite-sensitized solar cells. *Nature* 499, 316–319 (**2013**).

7. A. Kojima, K. Teshima, Y. Shirai, and T. Miyasaka. Organometal Halide Perovskites as Visible-Light Sensitizers for Photovoltaic Cells. *J. Am. Chem. Soc.* 131, 6050–6051 (**2009**).

8. M. Liu, M. B. Johnston, and H. J. Snaith. Efficient planar heterojunction perovskite solar cells by vapour deposition. *Nature* 501, 395–398 (**2013**).

9. T. A. Berhe, W.-N. Su, C.-H. Chen, C.-J. Pan, J.-H. Cheng, H.-M. Chen, M.-C. Tsai, L.-Y. Chen, A. A. Dubale, and B.-J. Hwang. Organometal halide perovskite solar cells: degradation and stability. *Energy Environ. Sci.* 9, 323–356 (**2016**).

10. P. P. Boix, S. Agarwala, T. M. Koh, N. Mathews, and S. G. Mhaisalkar. Perovskite Solar Cells: Beyond Methylammonium Lead Iodide. *J. Phys. Chem. Lett.* 6, 898–907 (**2015**).

11. B. Chen, M. Yang, S. Priya, and K. Zhu. Origin of J-V Hysteresis in Perovskite Solar Cells. *J. Phys. Chem. Lett.* 7, 905–917 (**2016**).

12. J. Chen, S. Zhou, S. Jin, H. Li, and T. Zhai. Crystal organometal halide perovskites with promising optoelectronic applications. *J. Mater. Chem. C* 4, 11–27 (**2016**).

13. P. Gao, M. Grätzel, and M. K. Nazeeruddin. Organohalide lead perovskites for photovoltaic applications. *Energy Environ. Sci.* 7, 2448 (**2014**).

14. G. Giorgi and K. Yamashita. Organic–inorganic halide perovskites: an ambipolar class of materials with enhanced photovoltaic performances. *J. Mater. Chem. A* 3, 8981–8991 (**2015**).

15. G. Giorgi and K. Yamashita. Zero-Dimensional Hybrid Organic-Inorganic Halide Perovskite Modeling: Insights from First Principles. *J. Phys. Chem. Lett.* 7, 888–899 (**2016**).

16. Y.-C. Hsiao, T. Wu, M. Li, Q. Liu, W. Qin, and B. Hu. Fundamental physics behind high-efficiency organo-metal halide perovskite solar cells. *J. Mater. Chem. A* 3, 15372–15385 (**2015**).

17. J. Huang, Y. Shao, and Q. Dong. Organometal Trihalide Perovskite Single Crystals: A Next Wave of Materials for 25% Efficiency Photovoltaics and Applications Beyond? *J. Phys. Chem. Lett.* 6, 3218–3227 (**2015**).

18. H. S. Jung and N.-G. Park. Perovskite Solar Cells: From Materials to Devices. *Small* 11, (**2014**).

19. M.-H. Li, P.-S. Shen, K.-C. Wang, T.-F. Guo, and P. Chen. Inorganic p-type contact materials for perovskite-based solar cells. *J. Mater. Chem. A* 3, 9011–9019 (**2015**).

20. S. Luo and W. A. Daoud. Recent progress in organic–inorganic halide perovskite solar cells: mechanisms and material design. *J. Mater. Chem. A* 3, 8992–9010 (**2015**).

21. A. R. Bin Mohd Yusoff and M. K. Nazeeruddin. Organohalide Lead Perovskites for Photovoltaic Applications. *J. Phys. Chem. Lett.* 7, 851–866 (**2016**).

22. G. Niu, X. Guo, and L. Wang. Review of Recent Progress in Chemical Stability of Perovskite Solar Cells. *J. Mater. Chem. A* 3, 8970–8980 (**2014**).

23. N.-G. Park. Perovskite solar cells: an emerging photovoltaic technology. *Mater. Today* 18, 65–72 (**2014**).

24. T. Salim, S. Sun, Y. Abe, A. Krishna, A. C. Grimsdale, and Y. M. Lam. Perovskite-based solar cells: impact of morphology and device architecture on device performance. *J. Mater. Chem. A* 3, 8943–8969 (**2015**).

25. J. Shi, X. Xu, D. Li, and Q. Meng. Interfaces in perovskite solar cells. *Small* 11, 2472–86 (**2015**).

26. S. Shi, Y. Li, X. Li, and H. Wang. Advancements in all-solid-state hybrid solar cells based on organometal halide perovskites. *Mater. Horiz.* 2, 378–405 (**2015**).

27. E. Singh and H. S. Nalwa. Graphene-Based Bulk-Heterojunction Solar Cells: A Review. *J. Nanosci. Nanotechnol.* 15, 6237–78 (**2015**).

28. E. Singh and H. S. Nalwa. Stability of graphene-based heterojunction solar cells. *RSC Adv.* 5, 73575–73600 (**2015**).

29. H. J. Snaith. Perovskites: The Emergence of a New Era for Low-Cost, High-Efficiency Solar Cells. *J. Phys. Chem. Lett.* 4, 3623–3630 (**2013**).

30. T.-B. Song, Q. Chen, H. Zhou, C. Jiang, H.-H. Wang, Y. (Michael) Yang, Y. Liu, J. You, and Y. Yang. Perovskite solar cells: film formation and properties. *J. Mater. Chem. A* 3, 9032–9050 (**2015**).

31. W. Wang, M. O. Tadé, and Z. Shao. Research progress of perovskite materials in photocatalysis- and photovoltaics-related energy conversion and environmental treatment. *Chem. Soc. Rev.* 44, 5371–408 (**2015**).

32. S. T. Williams, A. Rajagopal, C.-C. Chueh, and A. K.-Y. Jen. Current Challenges and Prospective Research for Upscaling Hybrid Perovskite Photovoltaics. *J. Phys. Chem. Lett.* 7, 811–819 (**2016**).

33. W. Yin, J. Yang, J. Kang, Y. Yan, and S.-H. Wei. Halide Perovskite Materials for Solar Cells: A Theoretical Review. *J. Mater. Chem. A* 3, 8926–8942 (**2014**).

34. Y. Zhao and K. Zhu. Solution Chemistry Engineering toward High-Efficiency Perovskite Solar Cells. *J. Phys. Chem. Lett.* 5, 4175–86 (**2014**).

35. F. Zheng, D. Saldana-Greco, S. Liu, and A. M. Rappe. Material Innovation in Advancing Organometal Halide Perovskite Functionality. *J. Phys. Chem. Lett.* 6, 4862–4872 (**2015**).

36. Y. Zhou, O. S. Game, S. Pang, and N. P. Padture. Microstructures of Organometal Trihalide Perovskites for Solar Cells: Their Evolution from Solutions and Characterization. *J. Phys. Chem. Lett.* 6, 4827–4839 (**2015**).

37. G. D. Scholes and G. Rumbles. Excitons in nanoscale systems. *Nat Mater* 5, 683–696 (**2006**).

38. I. Pelant and J. Valenta. Luminescence Spectroscopy of Semiconductors. Oxford Univ. Press (**2012**).

39. Q. Lin, A. Armin, R. C. R. Nagiri, P. L. Burn, and P. Meredith. Electro-optics of perovskite solar cells. *Nat Phot.* 9, 106–112 (**2015**).

40. M. A. Green, Y. Jiang, A. M. Soufiani, and A. Ho-Baillie. Optical Properties of Photovoltaic Organic–Inorganic Lead Halide Perovskites. *J. Phys. Chem. Lett.* 6, 4774–4785 (**2015**).

41. A. Miyata, A. Mitioglu, P. Plochocka, O. Portugall, J. T.-W. Wang, S. D. Stranks, H. J. Snaith, and R. J. Nicholas. Direct measurement of the exciton binding energy and effective masses for charge carriers in organic-inorganic tri-halide perovskites. *Nat. Phys.* 11, 582–587 (**2015**).

42. T. C. Sum and N. Mathews. Advancements in perovskite solar cells: photophysics behind the photovoltaics. *Energy Environ. Sci.* 7, 2518–2534 (**2014**).

43. G. Grancini, A. R. S. Kandada, J. M. Frost, A. J. Barker, M. De Bastiani, M. Gandini, S. Marras, G. Lanzani, A. Walsh, and A. Petrozza. Role of microstructure in the electron–hole interaction of hybrid lead halide perovskites. *Nat Phot.* 9, 695–701 (**2015**).

44. H.-S. Kim, S. H. Im, and N.-G. Park. Organolead Halide Perovskite: New Horizons in Solar Cell Research. *J. Phys. Chem. C* 118, 5615–5625 (**2014**).

45. K.-F. Lin, S. H. Chang, K.-H. Wang, H.-M. Cheng, K. Y. Chiu, K.-M. Lee, S.-H. Chen, and C.-G. Wu. Unraveling the high performance of tri-iodide perovskite absorber based photovoltaics with a non-polar solvent washing treatment. *Sol. Energy Mater. Sol. Cells* 141, 309–314 (**2015**).

46. N. Sestu, M. Cadelano, V. Sarritzu, F. Chen, D. Marongiu, R. Piras, M. Mainas, F. Quochi, M. Saba, A. Mura, and G. Bongiovanni. Absorption F-Sum Rule for the Exciton Binding Energy in Methylammonium Lead Halide Perovskites. *J. Phys. Chem. Lett.* 6, 4566–4572 (**2015**).

47. V. D'Innocenzo, G. Grancini, M. J. P. Alcocer, A. R. S. Kandada, S. D. Stranks, M. M. Lee, G. Lanzani, H. J. Snaith, and A. Petrozza. Excitons versus free charges in organo-lead tri-halide perovskites. *Nat Commun* 5, 582–587 (**2014**).

48. K. Zheng, Q. Zhu, M. Abdellah, M. E. Messing, W. Zhang, A. Generalov, Y. Niu, L. Ribaud, S. E. Canton, and T. Pullerits. Exciton Binding Energy and the Nature of Emissive States in Organometal Halide Perovskites. *J. Phys. Chem. Lett.* 6, 2969–2975 (**2015**).

49. T. C. Sum, S. Chen, G. Xing, X. Liu, and B. Wu. Energetics and dynamics in organic–inorganic halide perovskite photovoltaics and light emitters. *Nanotechnology* 26, 342001 (**2015**).

50. I. B. Koutselas, L. Ducasse, and G. C. Papavassiliou. Electronic properties of three- and low-dimensional semiconducting materials with Pb halide and Sn halide units. *J. Phys. Condens. Matter* 8, 1217 (**1996**).

51. T. J. Savenije, J. Carlito S. Ponseca, L. Kunneman, M. Abdellah, K. Zheng, Y. Tian, Q. Zhu, S. E. Canton, I. G. Scheblykin, T. Pullerits, A. Yartsev, and V. Sundström. Thermally Activated Exciton Dissociation and Recombination Control the Carrier Dynamics in Organometal Halide Perovskite. *J. Phys. Chem. Lett.* 5, 2189–2194 (**2014**).

52. V. D'Innocenzo, G. Grancini, M. J. P. Alcocer, A. R. S. Kandada, S. D. Stranks, M. M. Lee, G. Lanzani, H. J. Snaith, and A. Petrozza. Excitons versus free charges in organo-lead tri-halide perovskites. *Nat. Commun.* 5, 3586 (**2014**).

53. C. Wehrenfennig, G. E. Eperon, M. B. Johnston, H. J. Snaith, and L. M. Herz. High Charge Carrier Mobilities and Lifetimes in Organolead Trihalide Perovskites. *Adv. Mater.* 26, 1584–1589 (**2014**).

54. R. E. Wasylishen, O. Knop, and J. B. Macdonald. Cation rotation in methylammonium lead halides. *Solid State Commun.* 56, 581–582 (**1985**).

55. M. Hirasawa, T. Ishihara, T. Goto, K. Uchida, and N. Miura. Magnetoabsorption of the lowest exciton in perovskite-type compound $(CH_3NH_3)PbI_3$. *Phys. B Condens. Matter* 201, 427–430 (**1994**).

56. T. Ishihara. Optical properties of PbI-based perovskite structures. *J. Lumin.* 60-61, 269–274 (**1994**).

57. K. Tanaka, T. Takahashi, T. Ban, T. Kondo, K. Uchida, and N. Miura. Comparative study on the excitons in lead-halide-based perovskite-type crystals. *Solid State Commun.* 127, 619–623 (**2003**).

58. E. Menéndez-Proupin, C. L. B. Ríos, and P. Wahnón. Nonhydrogenic exciton spectrum in perovskite $CH_3NH_3PbI_3$. *Phys. status solidi – Rapid Res. Lett.* 9, 559–563 (**2015**).

59. C. C. Stoumpos, C. D. Malliakas, and M. G. Kanatzidis. Semiconducting Tin and Lead Iodide Perovskites with Organic Cations: Phase Transitions, High Mobilities, and Near-Infrared Photoluminescent Properties. *Inorg. Chem.* 52, 9019–9038 (**2013**).

60. A. Poglitsch and D. Weber. Dynamic disorder in methylammoniumtrihalogenoplumbates (II) observed by millimeter wave spectroscopy. *J. Chem. Phys.* 87, 6373–6378 (**1987**).

61. E. Menéndez-Proupin, P. Palacios, P. Wahnón, and J. C. Conesa. Self-consistent relativistic band structure of the $CH_3NH_3PbI_3$ perovskite. *Phys. Rev. B* 90, 45207 (**2014**).

62. E. Edri, S. Kirmayer, S. Mukhopadhyay, K. Gartsman, G. Hodes, and D. Cahen. Elucidating the charge carrier separation and working mechanism of $CH_3NH_3PbI_{3-x}Cl_x$ perovskite solar cells. *Nat Commun* 5 (**2014**).

63. J. Even, L. Pedesseau, and C. Katan. Analysis of Multivalley and Multibandgap Absorption and Enhancement of Free Carriers Related to Exciton Screening in Hybrid Perovskites. *J. Phys. Chem. C* 118, 11566–11572 (**2014**).

64. S. Sun, T. Salim, N. Mathews, M. Duchamp, C. Boothroyd, G. Xing, T. C. Sum, and Y. M. Lam. The origin of high efficiency in low-temperature solution-processable bilayer organometal halide hybrid solar cells. *Energy Environ. Sci.* 7, 399–407 (**2014**).

65. Y. Jiang, M. A. Green, R. Sheng, and A. Ho-Baillie. Room temperature optical properties of organic–inorganic lead halide perovskites. *Sol. Energy Mater. Sol. Cells* 137, 253–257 (**2015**).

66. Y. Jiang, M. A. Green, R. Sheng, and A. Ho-Baillie. Optical modelling data for room temperature optical properties of organic–inorganic lead halide perovskites. *Data Br.* 3, 201–208 (**2015**).

67. S. Taguchi, T. Goto, M. Takeda, and G. Kido. Magneto-Optical Effects of the Wannier Exciton in a Biaxial ZnP_2 Crystal. I. *J. Phys. Soc. Japan* 57, 3256–3261 (**1988**).

68. D. A. Valverde-Chavez, C. S. Ponseca, C. C. Stoumpos, A. Yartsev, M. G. Kanatzidis, V. Sundstrom, and D. G. Cooke. Intrinsic femtosecond charge generation dynamics in single crystal $CH_3NH_3PbI_3$. *Energy Environ. Sci.* (**2015**).

69. P. Piatkowski, B. Cohen, C. S. Ponseca Jr., M. Salado, S. Kazim, S. Ahmad, V. Sundstrom, and A. Douhal. Unraveling Charge Carriers Generation, Diffusion, and Recombination in Formamidiniurn Lead Triiodide Perovskite Polycrystalline Thin Film. *J. Phys. Chem. Lett.* 7, 204–210 (**2016**).

70. K. Galkowski, A. Mitioglu, atsuhiko miyata, paulina plochocka, oliver Portugall, G. E. Eperon, J. T.-W. Wang, T. Stergiopoulos, S. D. Stranks, H. Snaith, and R. J. Nicholas. Determination of the exciton binding energy and effective masses for methylammonium and formamidinium lead tri-halide perovskite semiconductors. *Energy Environ. Sci.* 9, 962–970 (**2016**).

71. R. Comin, G. Walters, E. S. Thibau, O. Voznyy, Z.-H. Lu, and E. H. Sargent. Structural, optical, and electronic studies of wide-bandgap lead halide perovskites. *J. Mater. Chem. C* 3, 8839–8843 (**2015**).

72. X. Deng, X. Wen, S. Huang, R. Sheng, T. Harada, T. W. Kee, M. A. Green, and A. W.-Y. Ho-Baillie. Ultrafast Carrier Dynamics in Methylammonium Lead Bromide Perovskite. *J. Phys. Chem. C* 120, (**2016**).

73. P. Piatkowski, B. Cohen, F. Javier Ramos, M. Di Nunzio, M. K. Nazeeruddin, M. Grätzel, S. Ahmad, and A. Douhal. Direct monitoring of ultrafast electron and hole dynamics in perovskite solar cells. *Phys. Chem. Chem. Phys.* 17, 14674–84 (**2015**).

74. V. Sharma, S. Aharon, I. Gdor, C. Yang, L. Etgar, and S. Ruhman. New insights into exciton binding and relaxation from high time resolution ultrafast spectroscopy of $CH_3NH_3PbI_3$ and $CH_3NH_3PbBr_3$ films. *J. Mater. Chem. a* 4, 3546–3553 (**2016**).

75. M. J. Simpson, B. Doughty, B. Yang, K. Xiao, and Y.-Z. Ma. Spatial Localization of Excitons and Charge Carriers in Hybrid Perovskite Thin Films. *J. Phys. Chem. Lett.* 6, 3041–3047 (**2015**).

76. Y. Yang, D. P. Ostrowski, R. M. France, K. Zhu, J. van de Lagemaat, J. M. Luther, and M. C. Beard. Observation of a hot-phonon bottleneck in lead-iodide perovskites. *Nat. Photonics* 10, 53–59 (**2016**).

77. S. D. Stranks, V. M. Burlakov, T. Leijtens, J. M. Ball, A. Goriely, and H. J. Snaith.

Recombination Kinetics in Organic-Inorganic Perovskites: Excitons, Free Charge, and Subgap States. *Phys. Rev. Appl.* 2, 034007 (**2014**).

78. S. Draguta, S. Thakur, Y. V Morozov, Y. Wang, J. S. Manser, P. V Kamat, and M. Kuno. Spatially Non-uniform Trap State Densities in Solution-Processed Hybrid Perovskite Thin Films. *J. Phys. Chem. Lett.* 7, 715–721 (**2016**).

79. J. Xing, X. F. Liu, Q. Zhang, S. T. Ha, Y. W. Yuan, C. Shen, T. C. Sum, and Q. Xiong. Vapor Phase Synthesis of Organometal Halide Perovskite Nanowires for Tunable Room-Temperature Nanolasers. *Nano Lett.* 15, 4571–4577 (**2015**).

80. S. T. Ha, X. Liu, Q. Zhang, D. Giovanni, T. C. Sum, and Q. Xiong. Synthesis of Organic–Inorganic Lead Halide Perovskite Nanoplatelets: Towards High-Performance Perovskite Solar Cells and Optoelectronic Devices. *Adv. Opt. Mater.* 2, 838–844 (**2014**).

81. Y. Yang, M. Yang, Z. Li, R. Crisp, K. Zhu, and M. C. Beard. Comparison of Recombination Dynamics in $CH_3NH_3PbBr_3$ and $CH_3NH_3PbI_3$ Perovskite Films: Influence of Exciton Binding Energy. *J. Phys. Chem. Lett.* 6, 4688–4692 (**2015**).

82. G. C. Papavassiliou and I. B. Koutselas. Structural, optical and related properties of some natural three- and lower-dimensional semiconductor systems. *Synth. Met.* 71, 1713–1714 (**1995**).

83. S. Wang, D. B. Mitzi, C. A. Feild, and A. Guloy. Synthesis and Characterization of $[NH_2C(I):NH_2]_3MI_5$ (M = Sn, Pb): Stereochemical Activity in Divalent Tin and Lead Halides Containing Single <110> Perovskite Sheets. *J. Am. Chem. Soc.* 117, 5297–5302 (**1995**).

84. G. C. Papavassiliou, I. B. Koutselas, A. Terzis, and M.-H. Whangbo. Structural and electronic properties of the natural quantum-well system $(C_6H_5CH_2CH_2NH_3)$_2SnI_4. *Solid State Commun.* 91, 695–698 (**1994**).

85. L. C. Schmidt, A. Pertegás, S. González-Carrero, O. Malinkiewicz, S. Agouram, G. M. Espallargas, H. J. Bolink, R. E. Galian, and J. Pérez-Prieto. Nontemplate Synthesis of CH_3NH_3PbBr_3 Perovskite Nanoparticles. *J. Am. Chem. Soc.* 136, 850–853 (**2014**).

86. D. Di, K. P. Musselman, G. Li, A. Sadhanala, Y. Ievskaya, Q. Song, Z.-K. Tan, M. L. Lai, J. L. MacManus-Driscoll, N. C. Greenham, and R. H. Friend. Size-Dependent Photon Emission from Organometal Halide Perovskite Nanocrystals Embedded in an Organic Matrix. *J. Phys. Chem. Lett.* 6, 446–450 (**2015**).

87. B. Luo, Y.-C. Pu, Y. Yang, S. A. Lindley, G. Abdelmageed, H. Ashry, Y. Li, X. Li, and J. Z. Zhang. Synthesis, Optical Properties, and Exciton Dynamics of Organolead Bromide Perovskite Nanocrystals. *J. Phys. Chem. C* 119, 26672–26682 (**2015**).

88. J. A. Sichert, Y. Tong, N. Mutz, M. Vollmer, S. Fischer, K. Z. Milowska, R. G. Cortadella, B. Nickel, C. Cardenas-Daw, J. K. Stolarczyk, A. S. Urban, and J. Feldmann. Quantum Size Effect in Organometal Halide Perovskite Nanoplatelets. *Nano Lett.* 15, 6521–6527 (**2015**).

89. O. Yaffe, A. Chernikov, Z. M. Norman, Y. Zhong, A. Velauthapillai, A. van der Zande, J. S. Owen, and T. F. Heinz. Excitons in ultrathin organic-inorganic perovskite crystals. *Phys.*

Rev. B 92, 45414 (**2015**).

90. F. Zhu, L. Men, Y. Guo, Q. Zhu, U. Bhattacharjee, P. M. Goodwin, J. W. Petrich, E. A. Smith, and J. Vela. Shape Evolution and Single Particle Luminescence of Organometal Halide Perovskite Nanocrystals. *ACS Nano* 9, 2948–2959 (**2015**).

91. S. González-Carrero, R. E. Galian, and J. Pérez-Prieto. Organometal Halide Perovskites: Bulk Low-Dimension Materials and Nanoparticles. *Part. Part. Syst. Charact.* 32, 709–720 (**2015**).

92. S. Gonzalez-Carrero, R. E. Galian, and J. Perez-Prieto. Maximizing the emissive properties of CH_3NH_3PbBr_3 perovskite nanoparticles. *J. Mater. Chem. A* 3, 9187–9193 (**2015**).

93. P. Tyagi, S. M. Arveson, and W. A. Tisdale. Colloidal Organohalide Perovskite Nanoplatelets Exhibiting Quantum Confinement. *J. Phys. Chem. Lett.* 6, 1911–1916 (**2015**).

94. E. Horváth, M. Spina, Z. Szekrényes, K. Kamarás, R. Gaal, D. Gachet, and L. Forró. Nanowires of Methylammonium Lead Iodide ($CH_3NH_3PbI_3$) Prepared by Low Temperature Solution-Mediated Crystallization. *Nano Lett.* 14, 6761–6766 (**2014**).

95. Z.-K. Tan, R. S. Moghaddam, M. L. Lai, P. Docampo, R. Higler, F. Deschler, M. Price, A. Sadhanala, L. M. Pazos, D. Credgington, F. Hanusch, T. Bein, H. J. Snaith, and R. H. Friend. Bright light-emitting diodes based on organometal halide perovskite. *Nat Nano* 9, 687–692 (**2014**).

96. H. Huang, F. Zhao, L. Liu, F. Zhang, X. Wu, L. Shi, B. Zou, Q. Pei, and H. Zhong. Emulsion Synthesis of Size-Tunable $CH_3NH_3PbBr_3$ Quantum Dots: An Alternative Route toward Efficient Light-Emitting Diodes. *ACS Appl. Mater. Interfaces* 7, 28128–28133 (**2015**).

97. H. Zhu, Y. Fu, F. Meng, X. Wu, Z. Gong, Q. Ding, M. V Gustafsson, M. T. Trinh, S. Jin, and X.-Y. Zhu. Lead halide perovskite nanowire lasers with low lasing thresholds and high quality factors. *Nat Mater* 14, 636–642 (**2015**).

98. Q. Zhang, S. T. Ha, X. Liu, T. C. Sum, and Q. Xiong. Room-Temperature Near-Infrared High-Q Perovskite Whispering-Gallery Planar Nanolasers. *Nano Lett.* 14, 5995–6001 (**2014**).

99. E. J. Juarez-Perez, R. S. Sanchez, L. Badia, G. Garcia-Belmonte, Y. S. Kang, I. Mora-Sero, and J. Bisquert. Photoinduced Giant Dielectric Constant in Lead Halide Perovskite Solar Cells. *J. Phys. Chem. Lett.* 5, 2390–2394 (**2014**).

100. J.-H. Im, J. Luo, M. Franckevičius, N. Pellet, P. Gao, T. Moehl, S. M. Zakeeruddin, M. K. Nazeeruddin, M. Grätzel, and N.-G. Park. Nanowire Perovskite Solar Cell. *Nano Lett.* 15, 2120–2126 (**2015**).